PROCEEDINGS OF SCIENCE

Recent results from LHCb

Alessia Satta*
INFN sez. Roma Tor Vergata
E-mail: alessia.satta@roma2.infn.it

The LHCb experiment at CERN Large Hadron Collider (LHC) will perform precision measurements of CP violating processes and rare decays of B mesons and other hadrons containing b or c quarks. In this contribution, first an overview of the main objectives of the LHCb experiment is given, then the LHCb performance and running experience from the first year of LHC operation is reported. Finally several early physics results are presented.

XLIX International Winter Meeting on Nuclear Physics, BORMIO2011
January 24-28, 2011
Bormio, Italy

*Speaker.

PoS(Bormio 2011)045

1. Introduction

The main goal of the LHCb experiment is the indirect search for New Physics through precision measurements of CP violating phases and rare decays of hadrons containing heavy quarks. Of particular interest are processes that are strongly suppressed in the Standard Model, such as flavour-changing neutral current $b \to s$ transitions. In these loop mediated processes, New Physics can lead to significant deviations from Standard Model predictions through additional amplitudes involving new heavy particles. These indirect searches extend the discovery potential for new particles to a mass range far beyond that accessible in direct searches. Moreover, observing the pattern of deviations from Standard Model predictions will give insights into the underlying dynamics of the New Physics and will permit the parameters of New Physics models to be constrained. The analysis strategies for six selected key measurements have been described in detail in the LHCb "roadmap" document [1]. They comprise measurements of the CKM angle γ from $B \to DK$ tree decays and from penguin-mediated charmless charged two-body B decays, the measurement of the B_s^0 $\overline{B}_s^0$ mixing phase ϕ_s, the determination of the branching fraction of the very rare decay $B_s^0 \to \mu^+\mu^-$, measurements of angular distributions in the rare decay $B^0 \to K^*\mu^+\mu^-$, and radiative $b \to s\gamma$ decays.

During the first year of data taking, 2010, the LHC delivered luminosity that was not yet sufficient to allow the key measurements to be performed. Nevertheless due to its unique η coverage, its excellent particle identification capabilities and the possibility to trigger on relatively low p_T particles, using the 2010 data LHCb had interesting opportunities for a wide range of measurements beyond its core physics programme. Some of them are reported in these proceedings.

2. The LHCb detector

To exploit best the strongly forward peaked $b\bar{b}$ production cross section at the LHC, the LHCb detector is laid out as a single-arm forward spectrometer. Its acceptance covers polar angles from 15 mrad to 300 mrad in the bending plane of the spectrometer magnet and 250 mrad in the non bending plane. This corresponds to a pseudo-rapidity coverage of about $1.9 < \eta < 4.9$. LHCb captures almost 40% of the $b\bar{b}$ production cross section at the LHC while covering only about 4% of the solid angle. An additional benefit of measuring at small polar angles is the possibility to set p_T trigger thresholds of ~ 1 GeV, which provides good efficiency for heavy flavour physics. A vertical cross section through the LHCb detector is shown in figure 1, a detailed description can be found in [2]. The detector consists of planar stations lined up along the LHC beam axis over a total length of about 20 m. A silicon micro-strip vertex detector (Vertex Locator) around the pp interaction region is followed by a first RICH detector, a tracking system comprising a single tracking station (TT) upstream of the 3.7 Tm dipole magnet and three tracking stations (T1-T3) downstream of the magnet, a second RICH detector, electromagnetic and hadronic calorimeters (SPD/PS, ECAL, HCAL) and finally a muon system (M1-M5). Key performance parameters are an excellent vertex resolution resulting in a proper time resolution of about 50 fs, a momentum resolution for charged particles of better than 0.5% up to above 100 GeV, good kaon/pion separation from 2 GeV up to 100 GeV, and an efficient trigger both for final states with leptons and for purely hadronic final states.

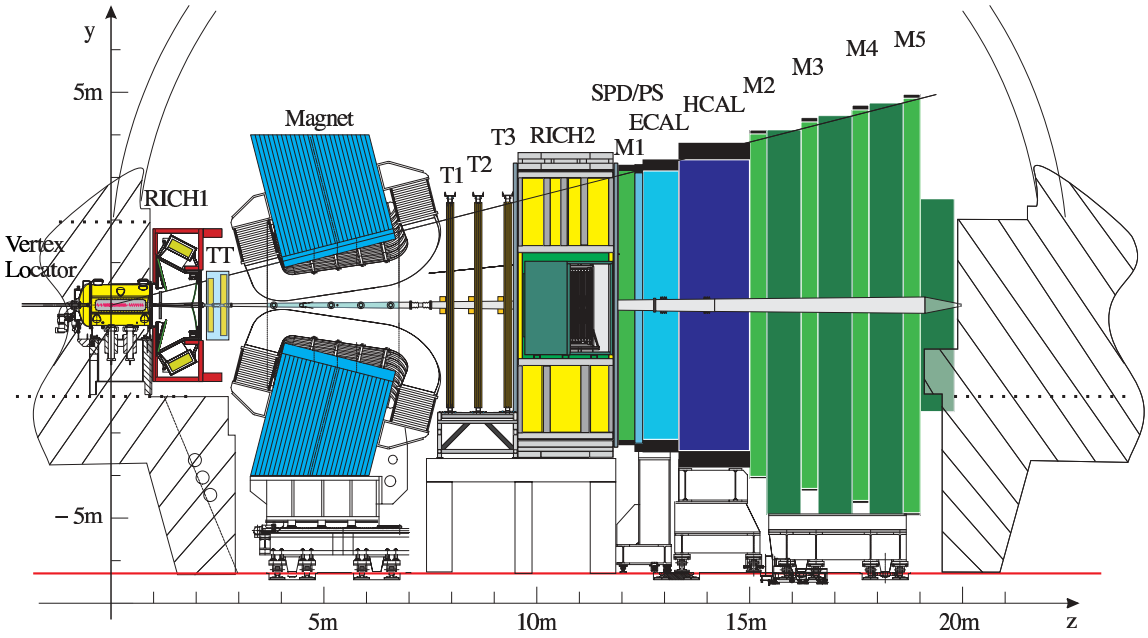

Figure 1: Vertical cross section through the LHCb detector. The pp collision point is in the centre of the Vertex Locator.

Another key element of the experiment is the trigger system: two levels reduce the rate from the 40 MHz input of the LHC clock to the 2 kHz output to the data acquisition. This is done exploiting fully the topology of B decays characterized by significant transverse momentum due to the high b quark mass and by long lifetime. The first level, called L0 (Level 0), is implemented in custom electronic boards working in a fully synchronous architecture with a fixed latency of 4 ms and a maximal output rate of 1 MHz. The calorimeters and the muon detectors are the main L0 contributors providing via dedicated electronics the highest momentum identified electron, photon, π^0, hadron, muon and di-muon candidates. The second level, called HLT (High Level Trigger), uses a farm of about 2000 central processing units. The HLT first reduces the rate to something like 30 kHz using the tracking information to confirm the L0 candidates, eventually adding an Impact Parameter (IP) cut. Only then inclusive and exclusive selections are built using the full event reconstruction.

3. Detector Performance and Running Experience

Except for the HLT computing farm, which was only partially installed, the LHCb experiment was fully operational from the first day of LHC collisions. About 37pb^{-1} of pp collisions at $\sqrt{s} =$ 7 TeV were collected during the 2010 LHC run, with a data taking efficiency of more than 90%. The polarity of the LHCb spectrometer magnet was reversed several times to minimize possible systematics due to detector asymmetries. LHC running conditions and the instantaneous luminosity provided by the accelerator evolved rapidly throughout the 2010 run. During the earliest runs, data were taken with a minimum-bias trigger. As the LHC luminosity increased, trigger conditions were gradually tightened such that the available readout bandwidth and CPU in the HLT farm were fully exploited. Data were taken at the highest luminosity available from LHC at all times, although

during the later part of the run this meant operating the experiment at significantly higher numbers of pp interactions per bunch crossing than foreseen under nominal conditions. Peak instantaneous luminosities close to the LHCb nominal luminosity were achieved towards the end of the 2010 run, but with only 344 instead of 2622 colliding bunches. These running conditions corresponded to an average number of visible interactions per bunch crossing, μ, of up to 2.4, where nominal LHCb operating conditions correspond to $\mu = 0.4$. A visible pp interaction is defined, here, as one that leaves signals in the LHCb detector. It was found that the detector and the reconstruction algorithms were much more robust in these harsh conditions than anticipated. The most significant limitation was found to be CPU time consumption in the not yet fully installed HLT farm for the reconstruction of very busy events. For some trigger lines, cuts on the maximum allowed number of hits in part of the tracking system and in one of the calorimeter sub-systems (SPD) were introduced to veto events with very high particle multiplicities when running at highest μ. The HLT farm has been completed over the 2010/2011 Christmas break. The positive experience from the 2010 creates the interesting option of operating the experiment at a higher than the initially foreseen instantaneous luminosity in 2011 and subsequent years.

An excellent vertex resolution is essential for the high-level trigger and for many physics analyses. To minimize extrapolation errors from the first measurement points to the vertex position, the LHCb vertex detector is installed inside the LHC vacuum vessel. The sensitive area of the detector starts at a distance of only 8 mm from the beam axis during data taking. The detectors have to be retracted by 3 cm during beam injection. They are moved into data taking position at the beginning of every fill when stable beams are declared. An internal alignment of better than 5 μm of the vertex detector has been obtained. Fill-to-fill variations in the position of the detectors are also as small as 5 μm. A single-hit resolution of 4 μm has been measured for the innermost readout strips. The measured track impact parameter resolution is slightly worse than expected from simulation; possible reasons for this are being investigated.

Excellent momentum and invariant mass resolutions are crucial for the rejection of combinatorial backgrounds. Measured spatial resolutions in the tracking system are approaching those expected from test beams and simulation. Small differences are remaining from residual misalignments. The acceptance of the LHCb tracking system for cosmics being negligibly small, its spatial alignment relies entirely on beam data. The good progress in the understanding of the alignment is demonstrated by the invariant mass resolution obtained for $J/\psi \to \mu^+\mu^-$ decays, which was 17.1 MeV in May 2010 and had reached 13.3 MeV by the end oof 2010. From simulation, an invariant mass resolution of 12.1 MeV is expected. Figure 2 shows a $\mu^+\mu^-$ invariant mass distribution in the mass range of the $\Upsilon(1S)$, $\Upsilon(2S)$ and $\Upsilon(3S)$ resonances. An invariant mass resolution of 47 MeV is obtained, here, and the three resonances are clearly resolved. Invariant mass distributions for a few $B \to J\psi X$ decay channels are shown in figure 3. Applying a mass constraint on the $J\psi$ mass, resolutions around 10 MeV are obtained for the B mass.

Another crucial ingredient for many analyses is an excellent kaon/pion separation over a wide momentum range. LHCb employs two RICH detectors incorporating three different radiators to cover momenta down to about 2 GeV, needed to identify kaons for B flavour tagging, and up to 100 GeV, required for a clean separation of two-body hadronic B decays. The particle-identification performance has been studied on data using tag-and-probe methods on $\phi \to K^+K^-$, $K^0_s \to \pi^+\pi^-$ and $\Lambda \to p\pi^-$ decays and is found to be close to expectations from simulation over the full momen-

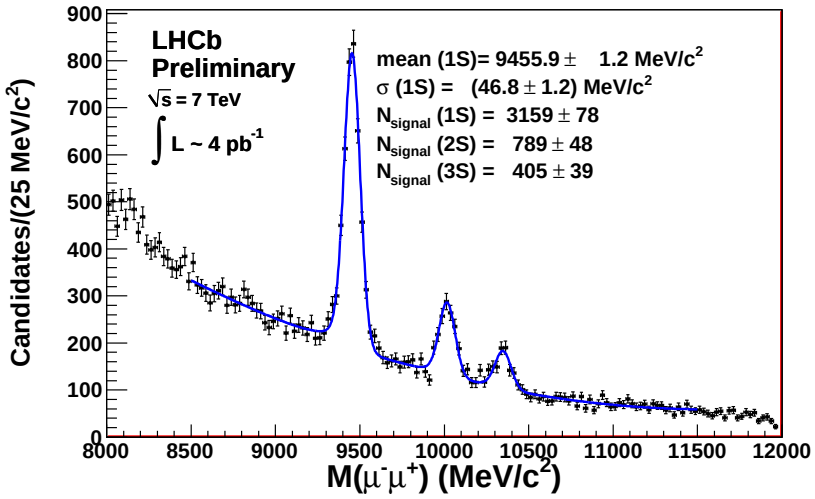

Figure 2: $\mu^+\mu^-$ invariant mass distribution showing the $\Upsilon(1S)$, $\Upsilon(2S)$ and $\Upsilon(3S)$ resonances. 4 pb^{-1} were used to obtain this distribution

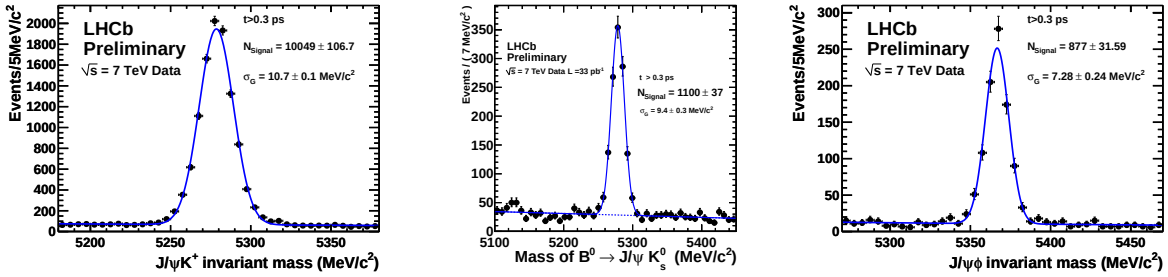

Figure 3: Invariant mass distributions for $B^+ \to J/\psi K^+$ (left), $B^0 \to J/\psi K^0_s$ (middle) and $B^0_s \to J/\psi\phi$ (right). A lifetime cut was applied on the B decay vertex to suppress combinatorial background. The J/ψ was reconstructed in the $\mu^+\mu^-$ final state and a mass constraint was applied on the J/ψ mass

tum range. The importance of kaon/pion separation for two-body hadronic B decays is illustrated in figure 4. The top left plot shows a $B \to h^+h^-$ invariant mass spectrum before particle-identification cuts, where the pion mass hypothesis was applied for both final-state particles. Despite the good invariant mass resolution, the contributions from $B^0 \to \pi^+\pi^-$, $B \to K^\pm\pi^\mp$ ans $B^0_s \to K^+K^-$ cannot be separated kinematically. The other three plots show invariant mass spectra for each of the three final states after particle-identification cuts have been applied. Clean signals with excellent invariant-mass resolution of 23 MeV are observed for all three decay modes. In the $K^\pm\pi^\mp$ final state, contributions from both B^0 and B^0_s can be seen.

Finally, the performance of the electromagnetic calorimeter in electron and photon reconstruction is illustrated in figure 5, which shows an e^+e^- invariant mass distribution with clear J/ψ and $\psi(2S)$ signals on the left and a $\chi_{c1;2} \to J/\psi\gamma$ signal on the right.

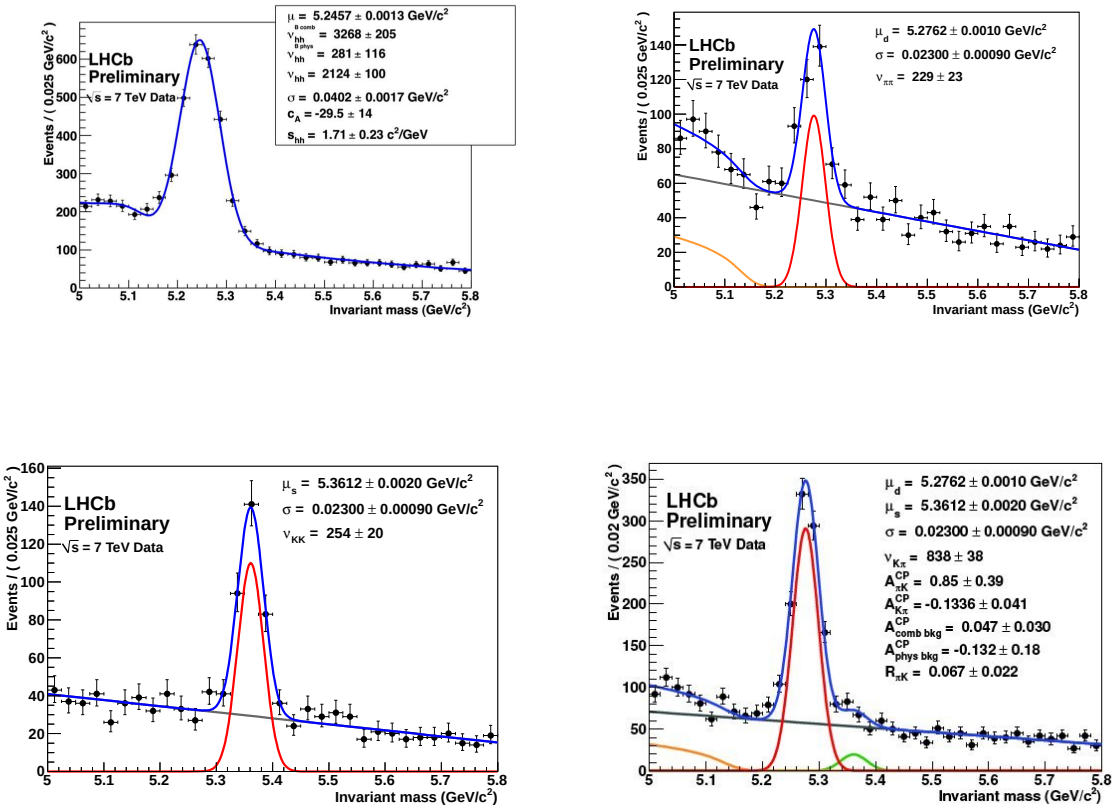

Figure 4: $B \to h^+h^-$ invariant mass distributions: before particle-identification, where the pion mass hypothesis was applied for both final-state particles (top left), and for $B^0 \to \pi^+\pi^-$ (top right),$B^0_s \to K^+K^-$ (bottom left) and $B^0_{d,s} \to K^\pm\pi^\mp$ (bottom right) after the application of loose kaon/pion identification criteria. The rising background at low invariant masses is due to mis-identified 3-body decays

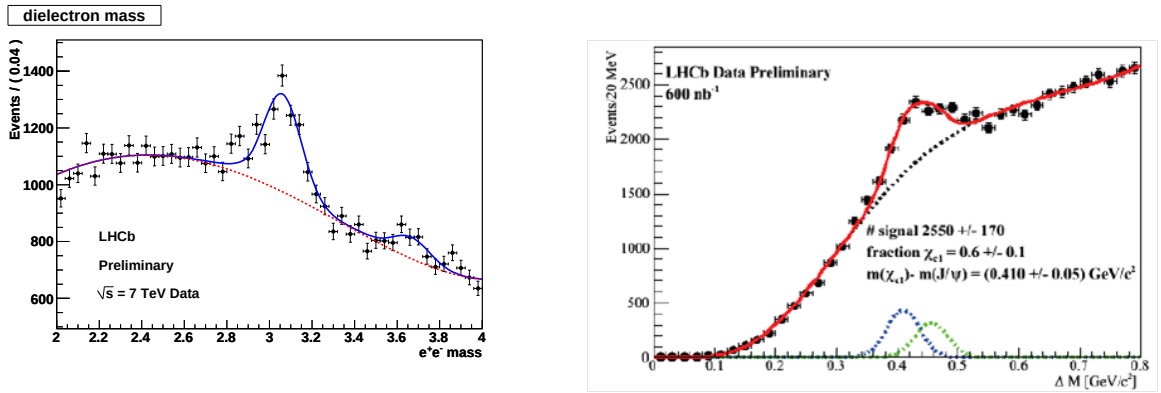

Figure 5: e^+e^- invariant mass distribution showing the J/ψ and $\psi(2S)$ resonances (left), $\chi_{c1;2} \to J/\psi(\mu^+\mu^-)\gamma$ signal (right). These distributions were obtained using only 1 pb^{-1} of data or less of measurements

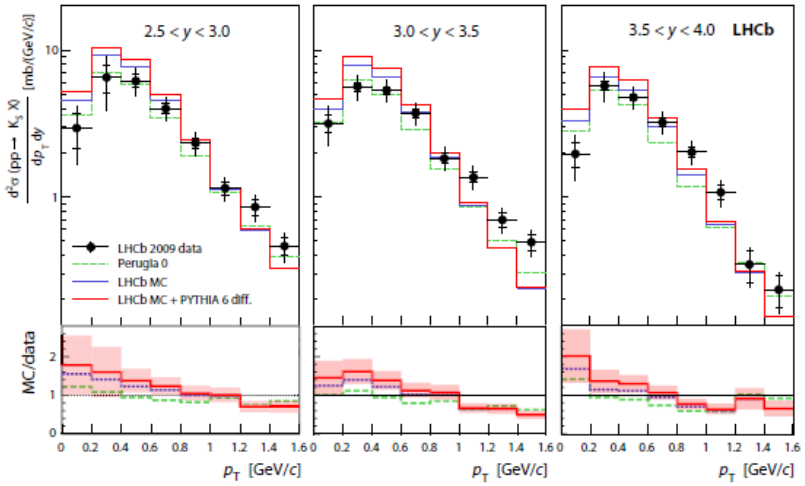

Figure 6: The prompt K_s^0 production cross section in pp collisions at $\sqrt{s} = 0.9$ TeV as a function of p_T and rapidity. Measurements are compared with the PYTHIA tuning Perugia0 [4] and the LHCb Monte Carlo (MC) with and without diffractive events.

4. Particle production studies

The measurements presented in this section are the production cross section of K_s^0 at $\sqrt{s} =$ 0.9 TeV, and the prompt $\overline{\Lambda}/\Lambda$, $\overline{\Lambda}/K_s^0$, and $\overline{p}/p$ production ratios and inclusive ϕ production cross section at $\sqrt{s} = 0.9$ TeV and $\sqrt{s} = 7$ TeV.

The results presented here are based on 6.8 nb^{-1} from the LHC 2009 pilot run at $\sqrt{s} = 0.9$ TeV, and 14 nb^{-1} accumulated by summer 2010 at $\sqrt{s} = 0.9$ TeV and $\sqrt{s} = 7$ TeV. These data-sets were recorded using minimum bias triggers, which require a minimum energy deposit in the LHCb calorimeters or at least one reconstructed track in the event. Due to the finite beam size and crossing angle, the two halves of the VELO were partially retracted during the $\sqrt{s} = 0.9$ TeV runs.

4.1 K_s^0 production

Strangeness production studies provide a valuable input to phenomenological models and in particular to the hadronisation mechanism. This is an ideal early measurement since K_s^0 are relatively abundant in minimum bias data and $K_s^0 \to \pi^+\pi^-$ candidates from the 2009 pilot run can be selected using only the tracking system. The results in figure 6 show a harder p_T spectrum than model predictions but are in good general agreement. Systematic uncertainties are dominated by the estimation of the integrated luminosity (12%) and tracking efficiency (10%). A detailed description of the analysis procedure and results are reported in [3].

4.2 V^0 production ratios

Another probe of strangess production is the measurement of the baryon versus meson suppression through the $\overline{\Lambda}/K_s^0$ production ratio. Moreover, the $\overline{\Lambda}/\Lambda$ ratio gives an estimate of the

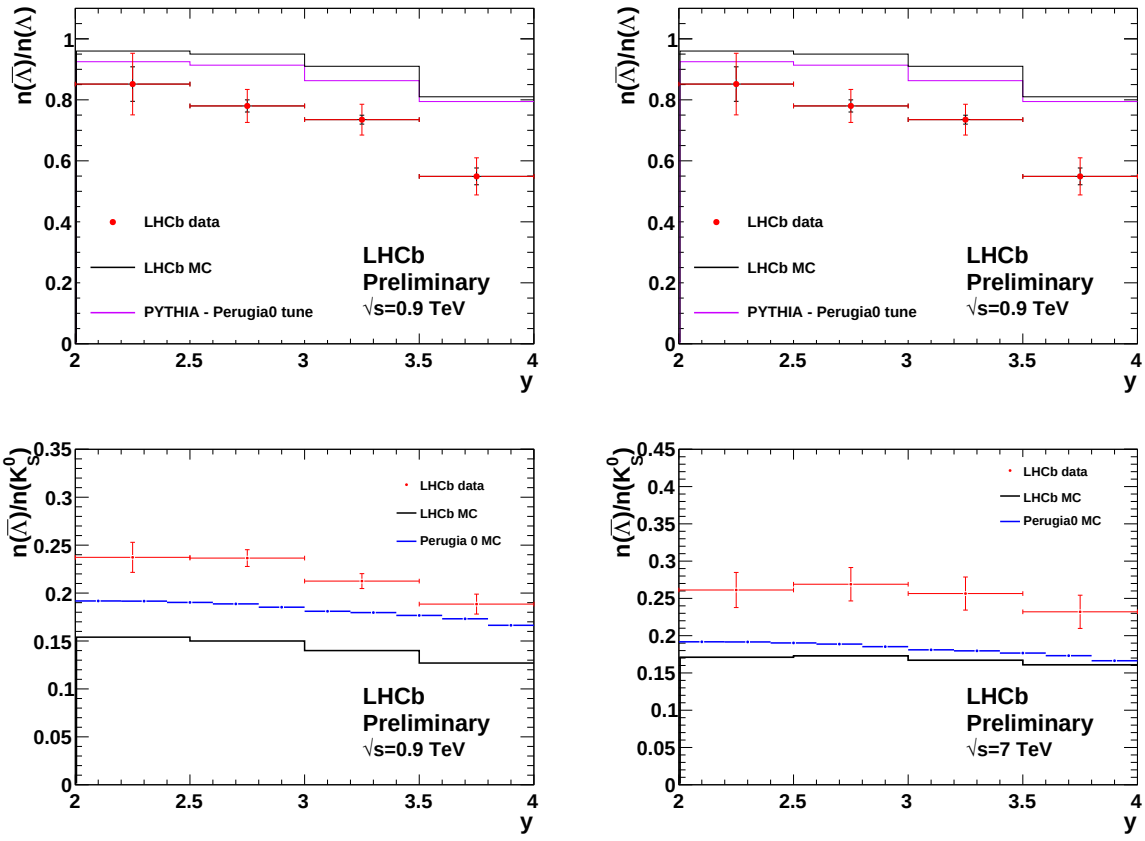

Figure 7: The prompt V^0 production ratio from pp collisions at $\sqrt{s} = 0.9$ TeV and $\sqrt{s} = 7$ TeV as a function of rapidity. The measurements are compared with the Perugia0 tuning and the LHCb MC. The error bars account for the total statistical and systematic uncertainty.

baryon number transport from the initial state protons to the final state products. High purity samples of $\Lambda(\overline{\Lambda}) \to p\pi^-(\overline{p}\pi^+)$ and $K^0_s \to \pi^-\pi^+$ are selected via a Fisher discriminant involving impact parameters with respect to the primary vertex. Preliminary results suggest that models underestimate the baryon number transport in $\overline{\Lambda}/\Lambda$ at $\sqrt{s} =$ 0.9 TeV and overestimate baryon suppression in $\overline{\Lambda}/K^0_s$ at both energies, as can be seen in figure 7. Since these measurements do not require the absolute luminosity, the systematic uncertainties are estimated to be relatively low, 2% for $\overline{\Lambda}/\Lambda$ and 2-12% for $\overline{\Lambda}/K^0_s$. The full analysis procedure and results are detailed in [5].

4.3 $\overline{p}/p$ production ratio

A further test of baryon number transport and hadronisation mechanisms is provided by the $\overline{p}/p$ production ratio. This analysis requires PID information from the RICH system in order to select pure samples of p, K and π. The RICH performance is calibrated using Λ, Φ , K^0_s decays reconstructed directly from data and this represents the main systematic uncertainty, particularly at high pseudorapidity. Preliminary results are consistent with MC predictions at $\sqrt{s} = 7$ TeV but differ significantly at $\sqrt{s} = 0.9$ TeV and low transverse momenta (see figure 8). Details of the analysis and results can be found in [6].

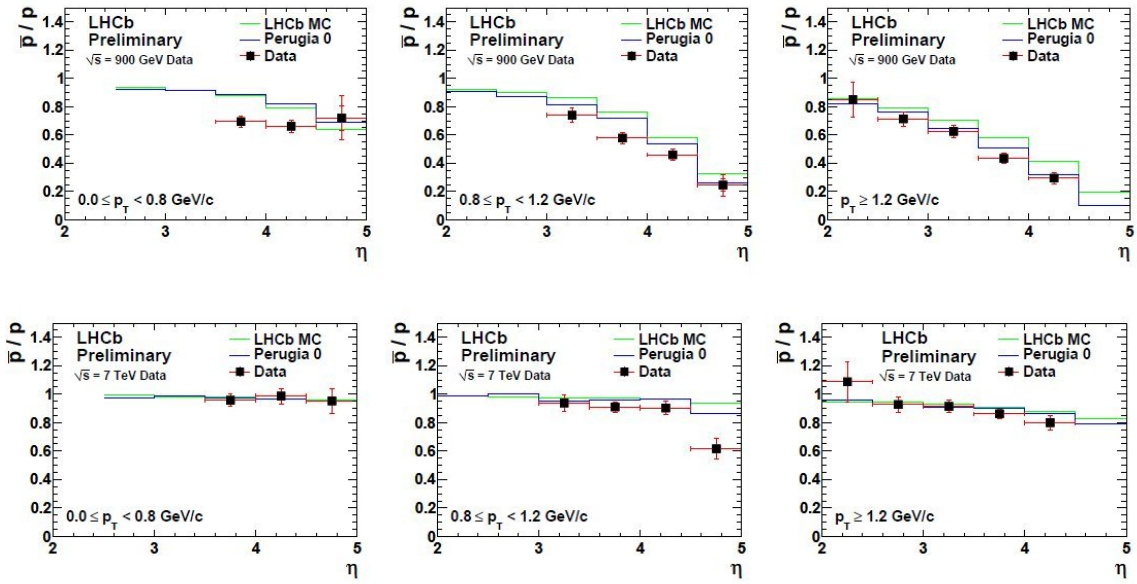

Figure 8: The prompt $\overline{p}/p$ production ratio from pp collisions at $\sqrt{s} = 0.9$ TeV and $\sqrt{s} = 7$ TeV as a function of pseudorapidity, η, in three bins of transverse momentum. The measurements are compared with the Perugia0 tuning and the LHCb MC. The error bars account for the total statistical and systematic uncertainty.

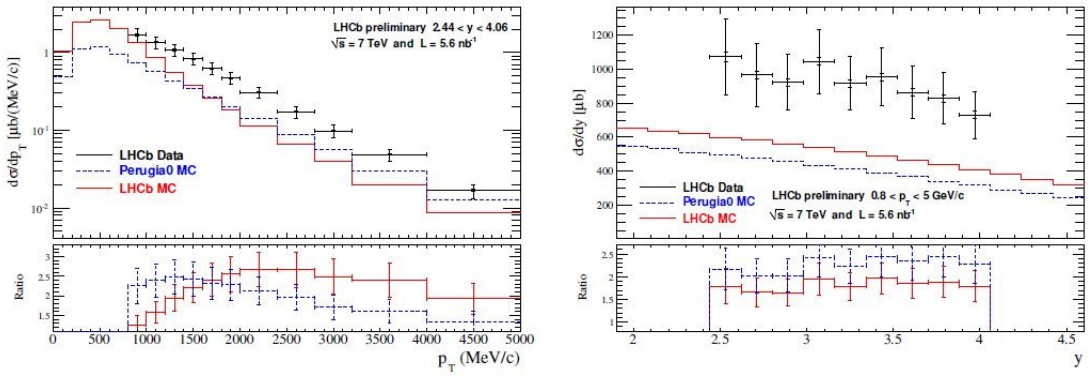

Figure 9: The prompt Φ production cross section from pp collisions at $\sqrt{s} = 7$ TeV as a function of rapidity and transverse momentum. The measurements are compared with the Perugia0 tuning and the LHCb MC.

4.4 Inclusive Φ production cross section

A further way to study strangeness production and to understand the hadronisation mechanism is the measurement of the Φ cross section. Like the $\overline{p}/p$ analysis, PID information from the RICH is required to select $\Phi \to K^+K^-$ candidates efficiently [6]. Preliminary results indicate a discrepancy from theoretical models, as shown in figure 9. As for the K^0_s cross section, the estimate of luminosity and tracking efficiency are the major systematic errors, the overall uncertainty is $\approx$ 14%.

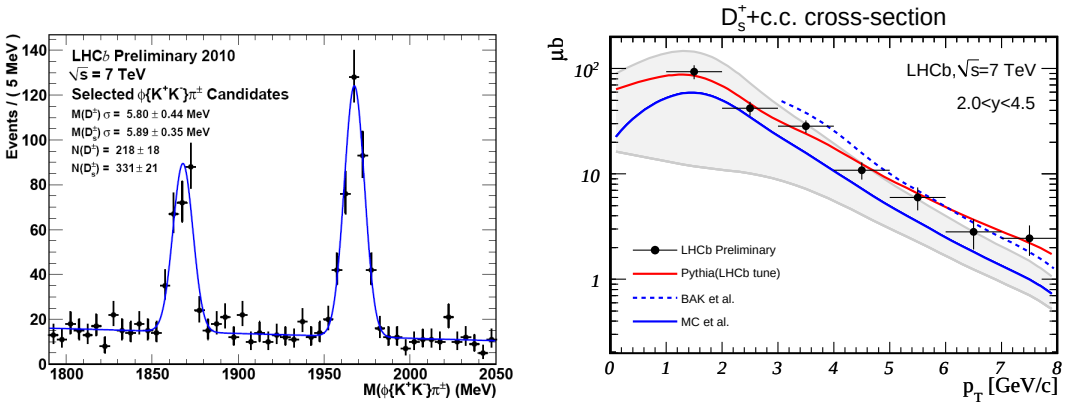

Figure 10: Invariant mass spectrum of the $\phi\pi$ candidates (left) and measured differential D_s production cross-section as a function of p_T (right). The shaded area indicates the uncertainties on the MC et al. prediction.

5. Open charm production

The open charm production has been studied on a data sample of 1.8 nb^{-1} collected with the microbias trigger. The production cross-sections of $D^0, \overline{D}^0, D^{*\pm}, D^{\pm}$ and $D_s^{\pm}$ have been determined in bins of transverse momentum and rapidity in the region $p_T < 8GeV/c$ and $2 < y < 4.5$ [7]. The decays channels used are: $D^0 \to K^-\pi^+$, $D^{*+} \to D^0(K^-\pi^+)\pi^+$, $D^+ \to K^-\pi^+\pi^-$, $D^+ \to \phi(K^+K^-)\pi^+$, $D_s^+ \to \phi(K^+K^-)\pi^+$, and their charge conjugates. For what concerns the D^+, the production cross section is obtained from the $K^-\pi^+\pi^-$ mode. The $\phi\pi^+$ mode is used to determine the cross-section ratio $\sigma(D^+)/\sigma(D_s^+)$. The prompt D are statistically separated from the D from b-flavoured hadron decays using the IP of the D candidate with respect to the closest primary vertex.

As an illustration, figure 10 shows two plots related to the $D_s^{\pm}$. The $D^{\pm}$ and $D_s^{\pm}$ peaks are clearly visible in the $\phi\pi^+$ invariant mass spectrum. The corresponding mass resolutions are smaller than 6 MeV/c^2. This is another example of the excellent performances of the tracking system. The measured p_T differential $D_s^{\pm}$ cross-section is compared with expectations from the LHCb tune of PYTHIA 6.4 and from QCD computations. Good agreements both in shape and in normalization are found. This statement is true for all the open charm cross-sections measured in this analysis. Extrapolating those measurements with PYTHIA 6.4 gives a $c\bar{c}$ production cross section in 4π: $\sigma(pp \to c\bar{c}X) = (6.10 \pm 0.93)$ mb.

6. J/ψ production cross-section

The J/ψ production has been studied on a sample of 14.2 nb^{-1} [8]. J/ψ of p_T up to 10 GeV/c and rapidity in the range $y \in [2.5;4]$ are considered. Figure 11 shows the invariant mass spectrum of the $J/\psi \to \mu^+\mu^-$ candidates. The distribution is fitted with a Crystal Ball function to describe the signal and a first order polynomial for the background. The inclusive J/ψ cross-section obtained from the fit is:

$$\sigma_{incJ/\psi}(p_t^{J/\psi} < 10GeV/c, 2.5 < y^{J/\psi} < 4) = (7.65 \pm .19 \pm 1.10^{+0.87}_{-1.27})\ \mu b,$$

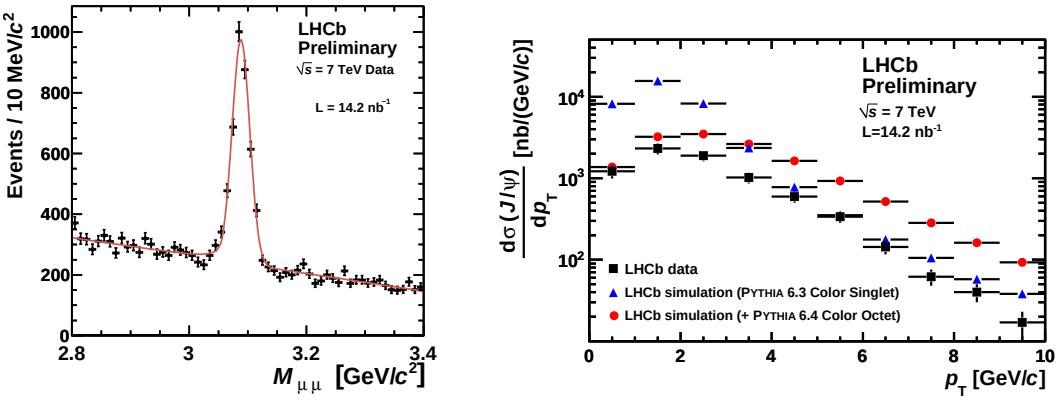

Figure 11: Invariant mass spectrum of the $J/\psi \to \mu^+\mu^-$ candidates (left) and measured differential inclusive J/ψ production cross-section as a function of p_T (right).

where the first error is statistical, the second one corresponds to systematic uncertainties, and the third one indicates the acceptance uncertainty due to the unknown J/ψ polarization. The systematic uncertainties are dominated by the uncertainty on the integrated luminosity (10%), followed by the uncertainty on the tracking efficiency (4% per muon track, i.e. a global effect of 8% here).

To measure the differential cross-section as a function of p_T, the J/ψ sample is divided in 10 sub-samples of 1 GeV/c in p_T. The $\mu^+\mu^-$ invariant mass distribution is then fitted in each sub-sample using the same functions as for the whole sample. The measured p_T differential cross-section is reported in figure 11, assuming non polarized J/ψ. The data is compared to two Monte Carlo models but none of them reproduce the measurements. Comparisons to more complete theoretical predictions are expected soon. To statistically separate J/ψ from b, which tend to be produced away from the primary vertex, from prompt J/ψ, produced immediately at the primary vertex, the pseudo-propertime along the z-axis is used. It is defined as:

$$tz = \frac{\Delta z \times M_{J/\psi}}{p_z},$$

where Δz is the distance along the z-axis between the J/ψ decay vertex and the closest primary vertex in the z direction, p_z is the measured J/ψ momentum in the z direction and $M_{J/\psi}$ the nominal J/ψ mass. Figure 12 shows the tz distribution. The data are fitted with three contributions: prompt J/ψ, J/ψ from b and background. The J/ψ from b cross-section obtained from the fit is:

$$\sigma_{J/\psi from b}(p_T^{J/\psi} < 10 GeV/c, 2.5 < y^{J/\psi} < 4) = (0.81 \pm 0.06 \pm 0.13)\ \mu b.$$

Extrapolations with PYTHIA 6.4 give an average cross-section to produce b-flavoured or $\bar{b}$-flavoured hadrons (H_b) with a pseudo-rapidity between 2 and 6 of[1].:

$$\sigma(pp \to H_b X, 2 < \eta(H_b) < 6) = (84.5 \pm 6.3 \pm 15.6)\ \mu b,$$

[1] At the time of this writing the analysis has been finalized using a larger dataset [9]

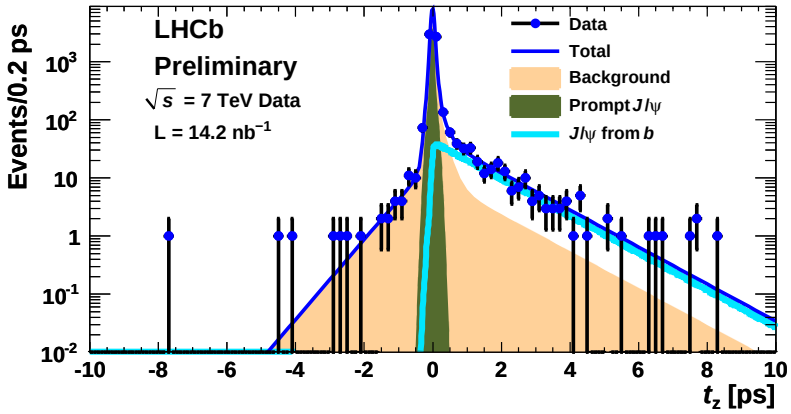

Figure 12: tz distribution of the J/ψ candidates.

and a $b\bar{b}$ production cross section in 4π of:

$$\sigma(pp \to b\bar{b}X) = (319 \pm 24 \pm 59)\ \mu b.$$

7. Beauty producion from $b \to D^0 X \mu^- \overline{\nu}_\mu$

Another way to measure the beauty production is to look at $b \to D^0 X \mu^- \overline{\nu}_\mu$ events [10]. This mode has a large branching fraction,$(6.84 \pm 0.35)\%$, and is advantageous from the point of view of signal to background. The analysis uses two independent data sets: a microbias sample and a muon trigger sample. The first comes from the earliest period of data taking and was recorded using the microbias trigger which is just requiring one track to be reconstructed. It corresponds to an integrated luminosity of 2.9 nb^{-1} . The second sample was recorded later with a single muon trigger and corresponds to an integrated luminosity of 12.2 nb^{-1}. The analysis uses the $D^0 \to K^-\pi^+$ decay mode which has a branching fraction of $(3.89 \pm 0.05)\%$ and yet is very clean. The D^0 from b-flavoured hadron decays are statistically separated from the prompt D^0 component thanks to the IP of the D^0 candidate with respect to the closest primary vertex. Distributions of the natural logarithm of the D^0 IP are presented in figure 13. These distributions corresponds to the muon trigger sample. They are presented separately for right-sign and wrong-sign candidates defined as the ones for which the charge of the muon and of the kaon from the $D^0$are the same or opposite, respectively. The semi-leptonic b decays mostly lead to right-sign candidates. The wrong-sign sample is then important to make sure the backgrounds are well modeled. In figure 13, the shape associated to the signal D^0 from b-flavoured hadron decays has been taken from the Monte Carlo. The one for the prompt D^0 background has been extracted from the microbias sample by considering candidates for which the track which is supposed to be associated to the muon fails the muon identification criteria. The shape from the non-D^0 background is obtained from the D^0 side-bands. The fit presented in figure 13 well reproduce the data both for right-sign and wrong-sign candidates.

As shown in figure 14, the average cross-section to produce b-flavoured or $\overline{b}$-flavoured hadrons is measured in four pseudo-rapidity bins. The LEP b hadronization fractions are used for the central

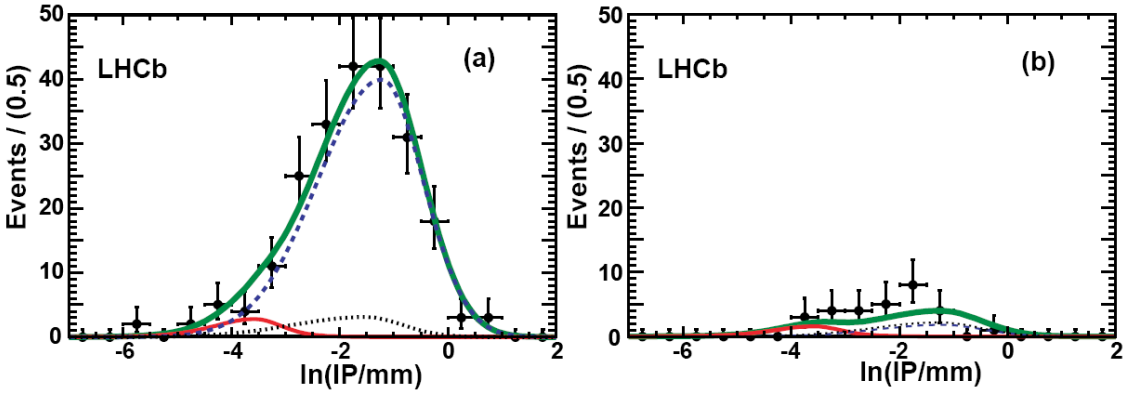

Figure 13: Natural logarithm of the D^0 IP for right-sign (left) and wrong-sign (right) D^0-muon candidates. The dashed curves represent D^0 from b-flavoured hadron decays, the thin solid curves the prompt D^0 component, the doted curves the non-D^0 background, and the thick solid curves the totals.

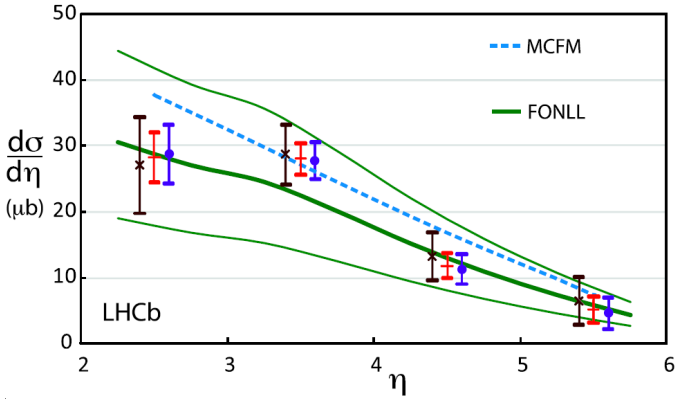

Figure 14: Measured differential b-flavoured hadron production crosssection as a function of η for the microbias sample (x), the muon triggered sample (•), and the average (+). The systematic uncertainties in the data are not included. The thin lines indicate the uncertainties on the FONLL prediction.

values. The results from the two independent data samples are compatible. Their combination is in good agreement with the theoretical predictions. Summing over the four pseudo-rapidity bins leads to the measurement:

$$\sigma(pp \to H_b X, 2 < \eta(H_b) < 6) = (75.3 \pm 5.4 \pm 13.0)\ \mu b.$$

Here also the systematic uncertainties are dominated by the uncertainty on the integrated luminosity (10%) and by the uncertainty on the tracking efficiency (3% for the kaon and the pion track, 4% for the muon track, i.e. a global effect of 10% here). An extrapolation with PYTHIA 6.4 gives in 4π

$$\sigma(pp \to b\bar{b}X) = (284 \pm 20 \pm 49)\ \mu b.$$

Those results are compatible with the one obtained from the J/ψ study. Combining them, using the LEP b hadronization fractions and extrapolating with PYTHIA 6.4, one obtains:

$$\sigma(pp \to H_b X, 2 < \eta(H_b) < 6) = (79.1 \pm 4.0 \pm 11.4)\ \mu b,$$

and:

$$\sigma(pp \to b\bar{b}X) = (298 \pm 15 \pm 43)\ \mu b.$$

8. Conclusions

The LHCb experiment has performed very well throughout the 2010 LHC run. About 37 pb^{-1} of data have been recorded, with a data taking efficiency in excess of 90%. A number of early analyses have demonstrated the ability of the LHCb detector to produce high quality results under harsher conditions than the experiment was designed for. Key performance parameters match or are close to expectations from simulation studies. Further improvements are still expected from better calibration and alignment. In several key analyses, sensitivities approaching those of existing measurements can already be expected from the 2010 data sample. With the much larger data sample expected for 2011, LHCb will be able to probe for New Physics signatures.

References

[1] B. Adeva et al. [LHCb Collaboration], "Roadmap for selected key measurements of LHCb", arxiv:0912.4179v2 [hep-ex]..

[2] A.A. Alves Jr. et al. [LHCb Collaboration], "The LHCb Detector at the LHC", 2008 JINST 3 S08005.

[3] The LHCb collaboration, Physics Letters B 683 (2010) 69.

[4] P.Z. Skands, CERN-PH-TH-2010-113.

[5] The LHCb collaboration, CERN-LHCb-CONF-2010-011.

[6] The LHCb collaboration, CERN-LHCb-CONF-2010-009.

[7] The LHCb Collaboration, CERN-LHCb-CONF-2010-013.

[8] The LHCb Collaboration, CERN-LHCb-CONF-2010-010.

[9] R. Aaij et al., [The LHCb Collaboration], CERN-PH-EP-2011-018, submitted to Eur. Phys. J. C.

[10] R. Aaij et al., [The LHCb Collaboration], Phys. Lett. B694 (2010) 209.